PHYSICAL REVIEW FLUIDS **1**, 051902(R) (2016)

Leidenfrost phenomenon on conical surfaces

S. Hidalgo-Caballero, Y. Escobar-Ortega, and F. Pacheco-Vázquez*
Instituto de Física, Benemérita Universidad Autónoma de Puebla, Apartado Postal J-48, Puebla 72570, Mexico

(Received 20 May 2016; published 26 September 2016)

The Leidenfrost state is typically studied by placing droplets on flat or slightly curved surfaces. Here this phenomenon is investigated by depositing water in hot conical bowls. We found that this phase exists even for large amounts of liquid in very narrow cones without considerable effect of the confinement on the Leidenfrost transition temperature T_L. At a fixed temperature, $T > T_L$, the total evaporation time τ has a nonmonotonic dependence on the angle of confinement θ: for large volumes ($\sim$20 ml) on flat surfaces ($\theta \sim 0^\circ$), vapor chimneys appear and accelerate the evaporation rate, their frequency diminishes as θ augments and becomes zero at a certain angle θ_c, at which τ reaches its maximum value; then, τ decreases again at larger angles because the vapor layer holding up the water becomes thinner due to the increase of hydrostatic pressure and because the geometry facilitates the vapor expulsion along the conical wall. For small volumes ($\sim$1 ml), surface tension mainly determines the drop curvature and the lifetime is practically independent of θ. Different chimney regimes and oscillation patterns were observed and summarized in a phase diagram. Finally, we developed a simple model to decipher the shape adopted by the liquid volume and its evolution as a function of time, and the predictions are in good agreement with the experimental results.

DOI: 10.1103/PhysRevFluids.1.051902

A liquid droplet deposited on a sufficiently hot surface levitates on its own vapor and evaporates slowly. Droplets with radius smaller than the liquid capillary length become spherical because surface tension prevails against gravity, whereas large drops are flattened by their own weight. The intermediate vapor layer avoids adhesive forces and suppresses friction, allowing the droplet to easily move on a horizontal flat plate.

The above phenomenon, called the Leidenfrost effect [1], has been conscientiously studied under different conditions of plate temperature [2,3], surface material [4], roughness and texture [5–8], ambient pressure [4,9], volume and purity of the liquid [10,11], etc. [12]. Different experimental techniques have been used to determine the drop shape and the thickness of the vapor layer [13,14], and various theoretical approaches have been also proposed [3,15–17]. Although the Leidenfrost phenomenon is typically studied by depositing liquids on solid surfaces, very recently it was addressed with drops deposited on liquid pools [18,19] and also with solids in sublimation [20,21]. Using a ratchet, a Leidenfrost droplet can be rotated as a turbine [21] or self-propelled in a well defined direction [22,23]. Nevertheless, in most of the studies the horizontal motion of the droplet was prevented using plates with a small curvature in order to analyze the evolution of the vapor layer and the shape of the droplet in the steady regime [3,13,16,17], or chimneys, star patterns, and other instabilities in the unsteady regime [14,24–27]. It has been mentioned that a larger curvature can suppress the Rayleigh-Taylor instability allowing considerable volumes of liquid to survive in Leidenfrost state [28–30]; however, the quantitative effect of lateral confinement on the liquid dynamics and on the evaporation process has not yet been addressed.

In this Rapid Communication, we study experimentally the Leidenfrost state of a large volume of water deposited on conical aluminum plates [see Figs. 1(a) and 1(b)]. Several regimes were observed

*Corresponding author: fpacheco@ifuap.buap.mx

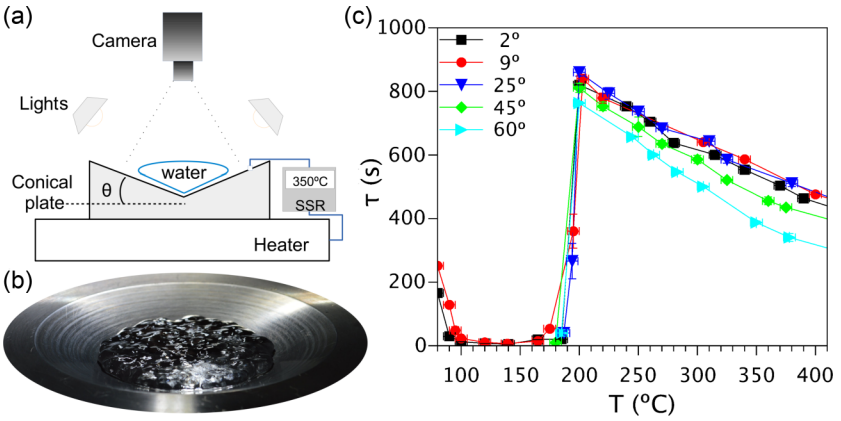

FIG. 1. (a) Experimental setup. (b) 20 ml of water preserving the Leidenfrost state on a conical surface of $\theta = 25^\circ$. (c) τ vs T for $V = 3$ ml; the angle of the conical surface does not affect the transition temperature T_L.

depending on the volume and angle of confinement. We found that the lifetime τ reaches a maximum value at a critical angle determined by the contact area and the competition of two mechanisms of vapor expulsion (lateral flow and chimneys). Furthermore, the shape adopted by the liquid volume on the plates, the thickness of the vapor layer, and the evolution of the drop as a function of time in stable conditions were numerically computed.

Experimental setup. Eleven solid aluminum cylinders of 15.0 ± 0.1 cm diameter were machined to produce conical bowls with angles $\theta = 1, 2, 3, 4, 6, 7.5, 9, 12, 25, 45$, and $60 \pm 0.5^\circ$. Each bowl was polished and cleaned to reduce the average roughness to less than 0.50 μm, as was verified using profilometry. Then, the bowl was placed on a hot plate connected to a solid-state relay temperature controller that allowed us to maintain the vertex of the cone at a constant temperature T ($\pm 10\,^\circ$C) with a decrease of $\sim$20 $^\circ$C along the edges. After waiting 20 min to stabilize the system temperature, a known volume of deionized water ranging from 0.5 up to 20 ml (the latter value limited by the dimensions of the bowls) was deposited on the conical surface and the process was filmed from the top at 30 fps until the liquid was totally evaporated. The evaporation time τ for the different volumes was measured from the videos and using a chronometer. Multiple regimes were observed and filmed from the top with a high speed camera at 1000 fps, and the videos were analyzed using ImageJ.

Figure 1(c) shows τ vs T in the range $90\,^\circ\text{C} < T < 400\,^\circ\text{C}$ for $V = 3.0 \pm 0.05$ ml and different angles. It is important to note that the Leidenfrost temperature is practically the same for all the bowls ($T_L \approx 195\,^\circ$C, within an error of 10 $^\circ$C), even for $\theta = 60^\circ$, indicating that lateral confinement is not relevant for this transition. This graph also indicates that, for fixed values of temperature and volume, τ varies with θ in a nonlinear manner. In what follows, we focus our study in the evaporation time, drop shape, and patterns observed for different volumes and angles at a fixed temperature value well above the Leidenfrost transition, and the case $\theta = 350 \pm 10\,^\circ$C was arbitrarily chosen.

Surface patterns. Figures 2(a)–2(d) show the evaporation process for $V = 20$ ml deposited on four different bowls of $\theta =$ (a) 2°, (b) 12°, (c) 25°, and (d) 45°. It is remarkable that the Leidenfrost state is maintained even with this large amount of water for very closed angles, where the hydrostatic pressure increases considerably. In fact, we did not find any limit for the angle or volume to observe the phenomenon. On the other hand, the surface dynamics viewed from the top is clearly affected by the angle of confinement, as shown in the snapshots. When $\theta \lesssim 9^\circ$, chimneys going through the water volume appear as a mechanism of vapor release; the number of chimneys decreases as the volume does, and they stop forming when oscillation modes start to show up. These modes evolve from ellipsoids to star shaped drops until they form a small spherical droplet, where surface tension principally determines its shape. For $\theta > 9^\circ$ the chimneys regime is no longer observed, indicating that the vapor is evacuated only laterally between the water and the side walls. The

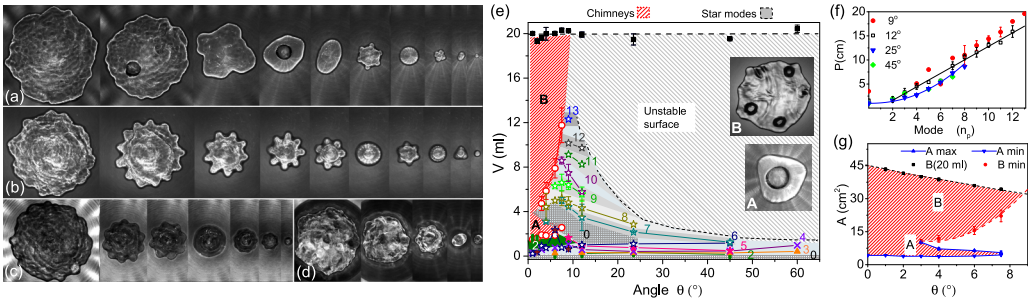

FIG. 2. Snapshots of the evaporation process of 20 ml of water deposited on conical bowls with $\theta = $ (a) 2°, (b) 12°, (c) 25°, and (d) 45°. (e) Phase diagram of the main regimes observed during the evaporation process: chimneys (A and B), unstable surface, and oscillation modes (n_p : 0–13). Embedded numbers indicate the corresponding star modes; for instance, 11 indicates a star of 11 peaks. (f) The perimeter of the star modes follows a linear (black) and a nonlinear dependence (blue) with n_p for small and large angles, respectively. (g) Two chimney regimes observed at small angles as mechanisms of vapor release: a unique central chimney (region A) generated by a Rayleigh-Taylor instability, and radial multichimneys (region B) where Kelvin-Helmholtz instabilities become important.

interfacial liquid-vapor interaction generates oscillating star modes of $n_p = 2$–13 peaks, which are more frequent and stable in the range from $\theta = 9^\circ$ to 12°. For larger angles, the Leidenfrost state still exists but fewer modes emerge and the surface is unstable [see Figs. 2(c) and 2(d)]. Figure 2(e) shows a phase diagram summarizing the different regimes based on the top view: chimneys for large volumes and open cones, unstable surface at large volumes and narrow cones, and a variety of oscillation modes depending on θ and V (to determine the volume of the observed modes we used calibration curves obtained by measuring the upper area A of known volumes for each angle). Note that the perimeter of the start modes follows a linear dependence with n_p for small angles [see Fig. 2(f)], in accordance with Ref. [30]; however, for larger angles a nonlinear relation was found, indicating a relevant influence of the surface curvature on the azimuthal wavelength of the oscillation modes.

One intriguing observation in the above phase diagram is the appearance of two different regimes of chimneys (see regions and snapshots labeled by A and B). High speed videos reveal that individual chimneys in region A arise when the drops are quasistable, while multichimneys in region B at larger volumes seem to have a turbulent origin. Our measurements indicate that the minimum upper area to observe chimneys has a constant value $A_{\min} \approx 3.94 \pm 0.27$ cm^2 [see Fig. 2(g)]. This area corresponds to an average critical radius $R_c \approx 1.12 \pm 0.04$ cm. Considering that the liquid-vapor interface is destabilized due to gravity (Rayleigh-Taylor instability) or due to the relative movement of the fluids (Kelvin-Helmholtz instability), we can neglect the second mechanism in region A and then apply the lubrication approximation to the Navier-Stokes equations. Under these conditions, the dynamic wavelength of the instability that is developed faster in a stable drop of radius r_s is given by $\lambda_{\rm dyn} = 2\pi\sqrt{2}a$, where $a = \sqrt{\gamma/\rho g} \approx 2.55$ mm is the capillary length, ρ and γ the density and surface tension of the liquid, and g the acceleration of gravity (see Ref. [14]). Since $\lambda_{\rm dyn} \approx 2r_s$ for small values of θ, the instability starts to appear when $r_s \approx 1.13$ cm, which is in excellent concordance with the value of R_c. This result indicates that chimneys in *region A* are mainly originated by a Rayleigh-Taylor instability. On the other hand, chimneys in *region B* appear in a more turbulent environment, where Kelvin-Helmhotz instabilities are important and the lubrication approximation is not valid. For this case, we found that the minimum area delimiting the region B increases nonlinearly with the angle [dashed red line in Fig. 2(g)], and for $V = 20$ ml chimneys can only be observed if $\theta \lesssim 8^\circ$.

Total evaporation time. Now let us analyze the effect of confinement on the total lifetime for $V = 20$ ml [see Fig. 3(a)]. As is shown, τ increases with θ and reaches a maximum value around $\theta_c \approx 8^\circ$.

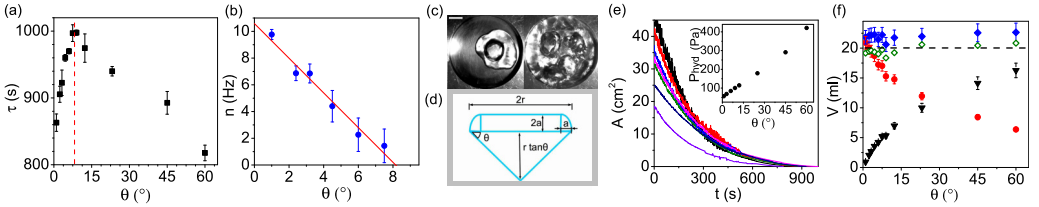

FIG. 3. (a) Evaporation lifetime τ vs θ for 20 ml of water at $T = 350\,^{\circ}$C; a maximum τ is reached when $\theta \approx 8^{\circ}$. (b) Sighting frequency of chimneys n as a function of θ for $V = 20$ ml; the linear fit (red line) indicates that $n = 0$ for $\theta = 8.2^{\circ}$. (c) Snapshots of chimneys emerging through 3 and 50 ml of water deposited on a cylindrical container of 5.5 cm diameter and 3 cm height (scale bar = 1 cm). For $V = 50$ ml, the hydrostatic pressure due to the water column is $P_{\mathrm{hyd}} \backsim 200$ Pa. (d) Sketch of the water distribution on a conical surface. (e) Evolution of the upper area A vs t during the evaporation of 20 ml of water deposited on conical plates with $\theta = 1^{\circ}, 3^{\circ}, 6^{\circ}, 9^{\circ}, 12^{\circ}, 25^{\circ}$, and 45°. Inset: P_{hyd} vs θ for $V = 20$ ml estimated at the vertex of the conical bowls. Note that chimneys emerge in the cylindrical geometry even when $P_{\mathrm{hyd}}^{\mathrm{cyl}} \gg P_{\mathrm{hyd}}^{\mathrm{cone}}(9^{\circ})$, revealing the relevance of the geometry. (f) Volume distribution calculated from the geometrical approach described in the text and sketched in (c): conical part (▼), puddle (●), total volume (◊), model (◊), and the experimental value of 20 ml (–).

Noteworthy, this range coincides with the chimney regime described in the phase diagram. Figure 3(b) shows the number of vapor chimneys per second n observed at the water surface as a function of θ for a constant volume; the red line represents the best linear fit $n = -(1.3 \pm 0.1)\theta + (10.6 \pm 0.4)$. Hence one finds that $n = 0$ when $\theta = 8.2^{\circ} \pm 1.1^{\circ}$, which is approximately the angle at which the maximum lifetime was measured. One possible explanation is that a chimney represents a mechanism of vapor release. If the chimneys disappear, the vapor only can escape laterally and the thickness of the vapor layer e increases, thus the heat transfer rate is reduced and τ rises; however, the competition with the hydrostatic pressure P_{hyd} becomes more important at larger angles, e decreases again and also the lifetime, which is in accordance with the experiment. In contrast, in a cylindrical container [see Fig. 3(c)] chimneys appear even for large volumes of liquid because the vapor cannot easily escape along the walls. Hence, two factors lead to a maximum lifetime and to the disappearance of chimneys: the vapor release favored by the geometry and the increase in hydrostatic pressure.

Shape. In order to calculate the evaporation rate and the dependence of e with θ it is necessary to determine the shape adopted by the water volume on the plates. According to Refs. [3,14,31], a large Leidenfrost drop on a flat surface is deformed by gravity and acquires a puddle shape of radius r (contac area πr^2) and thickness $h \approx 2a$. In the conical plates, our observations suggest that the volume is approximately distributed in a conical lower part crowned with a puddle [see sketch in Fig. 3(d)]. Considering that we can measure from the videos taken from the top the average upper area $A(t) = \pi r^2$ [see Fig. 3(e)], the volume can be approached by $V \approx V_{\mathrm{cone}} + V_{\mathrm{puddle}} = \frac{1}{3}\pi r^3 \tan\theta + \pi^2 a^2 (r - a) + 2\pi a (r - a)^2$, with the capillary length $a = 2.55$ mm. In Fig. 3(f) we plot the volume calculated with this geometrical approximation (◊) for experiments with 20 ml using $r = (A_{t=0}/\pi)^{1/2}$ obtained from Fig. 3(e). It is also shown the individual contributions of V_{cone} (▼) and V_{puddle} (●) to the total volume depending on θ. For small angles, the larger contribution is due to the puddle, but the conical part becomes more important as the angle gets larger. This approximation also allows one to estimate P_{hyd} as a function of θ at the bottom of the conical plates [see inset in Fig. 3(e)]. Nonetheless, although the geometric estimation is reasonably good, in all cases the addition of both volumes slightly overestimates the actual volume (20 ml, dashed line) due to the puddle shape; therefore, let us refine this contribution by computing numerically the puddle curvature.

Numerical approach. Let us take into account that the slope of the conical shape must smoothly match in a given point with the curvature of the upper puddle, as is sketched in Fig. 4(a). Based on Ref. [15], the pressure at the liquid-vapor interface $P(h) = P(0) + \rho g h$ is equilibrated by the

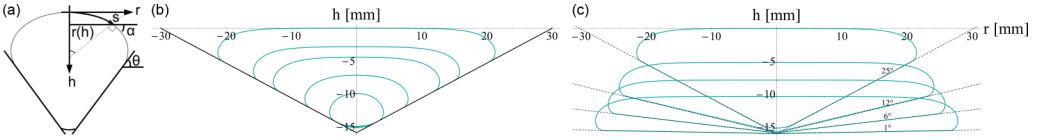

FIG. 4. (a) Sketch of a Leidenfrost drop on a conical surface; the lateral shape determined by the conical confinement was matched at the top (bottom) with the curvature determined by the balance of the Laplace pressure and the hydrostatic pressure. (b) and (c) Puddle profiles obtained by solving the curvature differential equations (see text) at (b) a constant angle $\theta = 25^\circ$ for $V = 0.2, 1, 3, 5, 10$ ml, and (c) a constant volume $V = 10$ ml with $\theta = 1^\circ, 6^\circ, 12^\circ$, and 25°.

Laplace pressure $P(h) = P_{\text{atm}} + \gamma(\frac{d\alpha}{ds} + \frac{\sin\alpha}{r}) = P_{\text{atm}} + \gamma\kappa(h)$, where $\kappa(h)$ determines the surface curvature at any depth h measured from the top of the liquid volume. Combining both expressions one finds $\gamma\kappa(h) = \rho g h + \gamma\kappa_0$, where κ_0 is the curvature at the top. By introducing the capillary length we can write $\kappa(h) = \frac{h}{a^2} + \kappa_0$, and then derive the differential equation: $\frac{d\alpha}{ds} = \kappa_0 + \frac{h}{a^2} - \frac{\sin\alpha}{r}$. On the other hand, from the geometry of the sketch in Fig. 4(a), we have $\frac{dr}{ds} = \cos\alpha$ and $\frac{dh}{ds} = \sin\alpha$. These three equations were numerically solved to obtain the upper puddle profile using the boundary conditions imposed by the volume and the bowl geometry, i.e., the matching of the drop curvature and the plate angle, $\alpha = \pi - \theta$. A similar analysis must be performed for the lower part with $\alpha = \theta$ considering the hydrostatic pressure at the bottom. Figure 4(b) shows the profiles for $\theta = 25^\circ$ using different values of $r(\alpha = \pi/2)$ calculated from the upper areas of known volumes (0.2, 1, 3, 5, and 10 ml), whereas Fig. 4(c) shows how the profile changes for different values of θ for a constant volume $V = 10$ ml. It is important to notice that the puddle thickness $h \approx 2a$ is recovered for a flat plate ($\theta = 1^\circ$). Moreover, the volume of solids of revolution calculated using numerical profiles better approximates the real volume $V = 20$ ml as is shown in Fig. 3(f) (◊), confirming the validity of our model.

Evaporation rate. In Ref. [3], it was found that the liquid evaporation rate can be expressed as $\dot{m} = \frac{K}{L}\frac{\Delta T}{e}A_c$ (E1), where K is the thermal conductivity of a vapor layer of thickness e, $\Delta T/e$ the temperature gradient, L the latent heat, and A_c the horizontal contact surface. In our case, $A_c = \pi r^2/\cos\theta$ is the conical face in contact with the liquid. On the other hand, by applying the lubrication approximation between the water volume and the conical surface one can estimate the vapor flux by $\dot{m} = \rho_v \frac{\pi e^3}{6\eta_v}\Delta P$, where $\Delta P = \rho_w g[h + r(h)\tan\theta]$ is the hydrostatic pressure as a function of r including the puddle and the conical part, ρ_v and ρ_w the density of vapor and water, respectively, and η_v the vapor dynamic viscosity; therefore, considering the average pressure on the conical wall one obtains $\dot{m} = \frac{\pi e^3 \rho_v \rho_w g}{6\eta_v}(2a + \frac{r}{4}\tan\theta)$. Equating both expressions of $\dot{m}$ and solving for the layer thickness, it is found that $e = (\frac{6\eta_v K \Delta T \sec\theta}{L\rho_v\rho_w g(2a + r\tan\theta/4)})^{1/4}\sqrt{r}$. Figure 5(a) shows $e(r)$ for different angles computed with the previous equation. Considering that A_c has a global minimum around $\theta \approx 40^\circ$ for a constant volume [see inset in Fig. 5(a)], we might have expected from (E1) a minimum heat transfer around this angle; however, because e depends on θ, our analysis reveals that the hydrostatic pressure plays a more important role decreasing the thickness of the vapor layer when θ grows, explaining why the lifetime diminishes in our experiments.

Finally, to find the evolution over time of a drop of volume V let us consider for simplicity the geometrical approximation described before in the mass change rate $\dot{m} = \rho_w \dot{V} = \rho_w \pi[4a(r - a) + \pi a^2 + \beta r^2 \tan\theta]\dot{r}$ (E2), with β a free parameter. Combining (E1) and (E2), and substituting e, one finds a differential equation for $r(t)$ that can be numerically integrated from an initial radius $r(t = 0) = r_0$ to $r(\tau) \approx 0$, and then use it to calculate $V(t)$ and τ for different values of θ. Figure 5(b) shows that the numerical solution (lines) describes fairly well the measured evolution (points) of $V(t)$ for different angles of confinement (all the cases fitted with the same value of β). Equivalently, Fig. 5(c) shows τ vs θ obtained from the numerical calculations compared with the experimental values for different initial volumes. As in most of the experiments, τ decreases as θ grows. At

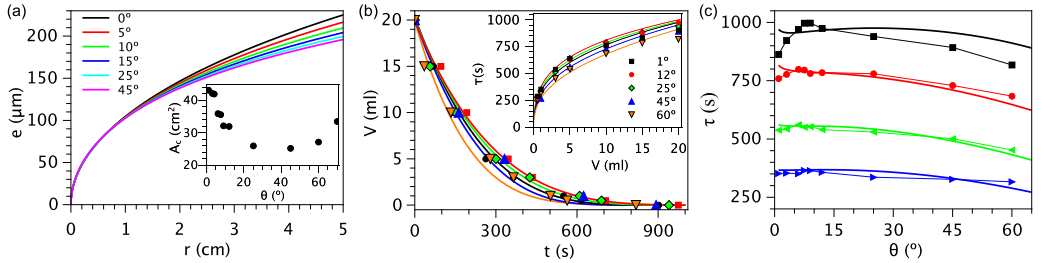

FIG. 5. (a) Thickness of the vapor layer e as a function of r for different angles. Inset: contact surface $A_c = \frac{\pi}{\cos\theta}(\frac{3V_{\text{cone}}}{\pi \tan\theta})^{2/3}$ corresponding to the data of the conical contribution in Fig. 3(e). (b) Evolution of the volume as a function of time starting from $V(t = 0) = 20$ ml; the inset shows the lifetime τ of known initial volumes V for different angles used to obtain the graph V vs t. (c) τ vs θ for volumes $V_0 = 1$ ml (▶), 5 ml (◀), 10 ml (●), and 20 ml (■). Solid lines in (b) and (c) are the numerical solutions of the model explained in the text.

large volumes and small angles, the model cannot describe the experimental points because of the appearance of chimneys, where the lubrication approximation cannot not be applied. Note that in the experimental data, the maximum lifetime is less notorious when the volume decreases because surface tension becomes more important against gravity and the plate curvature is less relevant. This maximum disappears only if the droplet is almost spherical, i.e., when its diameter is smaller than the capillary length.

Summarizing, we have studied the evaporation process of water deposited on conical bowls at temperatures larger than the Leidenfrost threshold. We found that T_L is not affected by the angle of confinement, and it was not detected any limit in this angle or a maximum liquid volume that can prevent the appearance of the phenomenon in the studied range. The evaporation time is determined by the dominant mechanism of vapor release, and a rich variety of surface patterns appear depending on the angle. We proposed a geometrical approximation to describe the shape acquired by the liquid inside the bowls and it was used to compute numerically the profiles and the evaporation dynamics. Our results reveal that, even when the surface curvature does not change the total evaporation time considerably, the confinement allows the controlled levitation of large volumes of liquid for a long time. Based on that, miniature Leidenfrost engines [21] can be scaled, and this can make possible low friction applications using confined structures. In addition, models to predict the origin of chimneys in the turbulent regime and their occurrence threshold are challenges that could attract the interest of the scientific community.

Acknowledgments. This research was supported by the projects: CONACyT Mexico No. 242085 of the Sectoral Research Fund for Education, PRODEP-SEP No. DSA/103.5/14/10819 and PROFOCIE-SEP 2015-2016. The authors would like to thank F. Moreau from Institut Pprime for valuable suggestions and enlightening discussions during the course of this work.

[1] J. G. Leidenfrost, *De Aquae Communis Nonullis Qualitatibus Tractatus* (Ovenius, Duisburg on Rhine, 1756).

[2] B. S. Gottfried, C. J. Lee, and K. J. Bell, The Leidenfrost phenomenon: Film boiling of liquid droplets on a flat plate, Int. J. Heat Mass Transfer **9**, 1167 (1966).

[3] A.-L. Biance, C. Clanet, and D. Quéré, Leidenfrost drops, Phys. Fluids **15**, 1632 (2003).

[4] G. S. Emmerson, The effect of pressure and surface material on the Leidenfrost point of discrete drops of water, Int. J. Heat Mass Transfer **18**, 381 (1975).

[5] C. Kruse, T. Anderson, C. Wilson, C. Zuhlke, D. Alexander, G. Gogos, and S. Ndao, Extraordinary shifts of the Leidenfrost temperature from multiscale micro/nanostructured surfaces, Langmuir **29**, 9798 (2013).

[6] H. Kim, B. Truong, J. Buongiorno, and L.-W. Hu, On the effect of surface roughness height, wettability, and nanoporosity on Leidenfrost phenomena, Appl. Phys. Lett. **98**, 083121 (2011).
[7] J. D. Bernardin and I. Mudawar, A cavity activation and bubble growth model of the Leidenfrost point, J. Heat Transfer **124**, 864 (2002).
[8] I. U. Vakarelski, N. A. Patankar, J. O. Marston, D. Y. C. Chan, and S. T. Thoroddsen, Stabilization of Leidenfrost vapour layer by textured superhydrophobic surfaces, Nature (London) **489**, 274 (2012).
[9] D. Orejon, K. Sefiane, and Y. Takata, Effect of ambient pressure on Leidenfrost temperature, Phys. Rev. E **90**, 053012 (2014).
[10] C.-K. Huanga and V. P. Careyb, The effects of dissolved salt on the Leidenfrost transition, Int. J. Heat Mass Transfer **50**, 269 (2007).
[11] G. Paul, D. P. K. Das, and I. Manna, Droplet oscillation and pattern formation during Leidenfrost phenomenon, Exp. Thermal Fluid Sci. **60**, 346 (2015).
[12] See a complete review of the topic by D. Quéré, Leidenfrost dynamics, Annu. Rev. Fluid Mech. **45**, 197 (2013).
[13] J. C. Burton, A. L. Sharpe, R. C. A. van der Veen, A. Franco, and S. R. Nagel, Geometry of the Vapor Layer Under a Leidenfrost Drop, Phys. Rev. Lett. **109**, 074301 (2012).
[14] A.-L. Biance, *Gouttes inertielles: de la caléfaction a l'étalement* (Physique des liquides, Université de Paris IV, 2003).
[15] K. Piroird, *Dynamiques speciales de gouttes non-mouillantes* (Mateire Molle, Ecole Polytechnique X, 2011).
[16] Y. Pomeau, M. Le Berre, F. Celestini, and T. Frisch, The Leidenfrost effect: From quasi-spherical droplets to puddles, C. R. Mecanique **340**, 867 (2012).
[17] B. Sobac, A. Rednikov, S. Dorbolo, and P. Colinet, Leidenfrost effect: Accurate drop shape modeling and refined scaling laws, Phys. Rev. E **90**, 053011 (2014).
[18] L. Maquet, B. Sobac, B. Darbois-Texier, A. Duchesne, M. Brandenbourger, A. Rednikov, P. Colinet, and S. Dorbolo, Leidenfrost drops on a heated liquid pool, arXiv:1603.05821v2 [Phys. Rev. Fluids (to be published)].
[19] M. Adda-Bedia, S. Kumar, F. Lechenault, S. Moulinet, M. Schillaci, and D. Vella, Inverse Leidenfrost effect: Levitating drops on liquid nitrogen, Langmuir **32**, 4179 (2016).
[20] S. Dorbolo, N. Adami, C. Dubois, H. Caps, N. Vandewalle, and B. Darbois-Texier, Rotation of melting ice disks due to melt fluid flow, Phys. Rev. E **93**, 033112 (2016).
[21] G. G. Wells, R. Ledesma-Aguilar, G. McHale, and K. Sefiane, A sublimation heat engine, Nat. Commun. **6**, 6390 (2015).
[22] H. Linke, B. J. Alemán, L. D. Melling, M. J. Taormina, M. J. Francis, C. C. Dow-Hygelund, V. Narayanan, R. P. Taylor, and A. Stout, Self-Propelled Leidenfrost Droplets, Phys. Rev. Lett. **96**, 154502 (2006).
[23] G. Lagubeau, M. Le Merrer, C. Clanet, and D. Quéré, Leidenfrost on a ratchet, Nat. Phys. **7**, 395 (2011).
[24] P. S. Raux, G. Dupeux, C. Clanet, and David Quéré, Successive instabilities of confined Leidenfrost puddles, Europhys. Lett. **112**, 26002 (2015).
[25] G. Paul, I. Manna, and P. K. Das, Formation, growth, and eruption cycle of vapor domes beneath a liquid puddle during Leidenfrost phenomena, Appl. Phys. Lett. **103**, 084101 (2013).
[26] N. J. Holter and W. R. Glasscock, Vibrations of evaporating liquid drops, J. Acoust. Soc. Am. **24**, 682 (1952).
[27] P. Casal and H. Gouin, Vibrations of liquid drops in film boiling phenomena: The mathematical model, Int. J. Eng. Sci. **32**, 1553 (1994).
[28] S. Perrard, Y. Couder, E. Fort, and L. Limat, Leidenfrost levitated liquid tori, Europhys. Lett. **100**, 54006 (2012).
[29] S. Perrard, L. Deike, C. Duchêne, and C.-T. Pham, Capillary solitons on a levitated medium, Phys. Rev. E **92**, 011002(R) (2015).
[30] X. Ma, J. J. Liétor-Santos, and J. C. Burton, The many faces of a Leidenfrost drop, Phys. Fluids **27**, 091109 (2015).
[31] P.-G. DeGennes, F. Brochard-Wyart, and D. Quéré, *Capillarity and Wetting Phenomena* (Springer, New York, 2003).